PCCP

PAPER

View Article Online
View Journal | View Issue

Cite this: *Phys. Chem. Chem. Phys.*, 2015, **17**, 6874

Electrical percolation thresholds of semiconducting single-walled carbon nanotube networks in field-effect transistors

Ho-Kyun Jang, Jun Eon Jin, Jun Hee Choi, Pil-Soo Kang, Do-Hyun Kim* and Gyu Tae Kim*

Received 19th December 2014,
Accepted 27th January 2015

DOI: 10.1039/c4cp05964f

www.rsc.org/pccp

With the advances in the separation and purification of carbon nanotubes (CNTs), the use of highly pure metallic or semiconducting CNTs has practical merit in electronics applications. When highly pure CNTs are applied in various fields, CNT networks are preferred to individual CNTs. In such cases, the presence of an electrical path becomes crucial in the network. In this study, we report on the electrical percolation thresholds of semiconducting single-walled carbon nanotube (s-SWCNT) networks, and their electrical characteristics in field-effect transistors (FET). Using the Monte Carlo method, s-SWCNT networks were randomly generated in the channels defined by the source–drain electrodes of the FET. On the basis of percolation theory, the percolation thresholds of s-SWCNT networks were obtained at different channel lengths (2, 6, and 10 μm) by generating random s-SWCNT networks 100 times. The network density corresponding to the electrical percolation threshold was theoretically gained at each channel length. As a result, the network densities at the percolation thresholds for the channel lengths of 2, 6, and 10 μm were 6.8, 9.0, and 9.9 tube μm^{-2}, respectively. In addition, SPICE calculations were performed for each s-SWCNT network, constituting an electrical path between the source and the drain electrodes of the FET. In all channel lengths, the on/off ratio of the s-SWCNT networks was enhanced with increasing network density. Finally, we found a power law relationship between the on/off ratio of the s-SWCNT networks and the network density at the percolation threshold.

Introduction

Carbon nanotubes (CNTs) have received much attention as an electronic material since their discovery in 1991, due to their outstanding electrical properties.[1,2] In general, it is known that according to their chirality, the electrical properties of CNTs can be classified into two types: metallic and semiconducting CNTs.[3–7] Depending on their applications, CNTs can be used in various fields, such as organic light-emitting diodes, transparent conductive films, and solar cells.[8–10] In these cases, CNT networks are preferred to individual CNTs. This is because treating CNTs as a structure of networks is convenient for further applications, compared with individual CNTs.

Currently, it is possible to obtain highly pure semiconducting or metallic CNTs, by virtue of progressive advances in CNT separation techniques. Single-walled carbon nanotubes (SWCNTs) have been sorted by diverse methods, such as sequence-dependent DNA assembly, gel-based separation, and density differentiation.[11–13] Moreover, the direct synthesis of semiconducting SWCNTs (s-SWCNTs) has been reported.[14] These methods have stimulated the use of CNT electronics in basic and applied fields.

When CNTs are utilized in electronics in the form of networks, an essential issue is the presence of an electrical path, which consists of individual semiconducting or metallic CNTs in the networks. Much effort has been made to study electrical percolation in CNT networks, based on the Monte Carlo method.[15–20] This approach can contribute to the discovery of optimal conditions when creating CNT networks. Sangwan and co-workers optimized the transistor performance of percolating CNT networks with the help of Monte Carlo simulations.[18] Moreover, this approach can predict the effect of CNT vacancy defects on the electrical characteristics when the network is composed of defective CNTs. Berahman *et al.* calculated that CNTs with double vacancies decrease the electrical conductivity of the percolated CNT network.[20] Furthermore, theoretical work can calculate the electrical characteristics of CNT networks, which have different ratios of metallic and semiconducting CNTs. This can provide a guideline for the design of experimental conditions to prepare CNT networks. In spite of laborious efforts to study CNT percolation, most of the studies have focused on multi-walled CNT or SWCNT networks where s-SWCNTs exist with metallic SWCNTs

School of Electrical Engineering, Korea University, Anam-dong, Seongbuk-gu, 136-713 Seoul, Korea. E-mail: nanotube@korea.ac.kr; Tel: +82-2-3290-3801

(m-SWCNTs) at the same time. The percolation thresholds of s-SWCNT networks have not been reported. In addition, few previous works have studied the electrical characteristics of percolated CNT networks. This motivated us to obtain the percolation threshold of s-SWCNTs and relate it to their electrical characteristics.

In this study, we report on the electrical percolation thresholds of s-SWCNT networks formed in the channel of field-effect transistors (FET), and the electrical characteristics of percolated networks, using a SPICE simulator. Currently, there are a number of experimental reports where highly pure s-SWCNT networks have been constituted between the source and drain electrodes on FETs for various purposes.[21–28] In the constitution of s-SWCNT networks with impure m-SWCNT, we cannot expect semiconducting behaviour from the dense s-SWCNT networks due to metallic paths in the networks. To avoid this, information on the critical network density of s-SWNCTs is required. However, to the best of our knowledge, the critical number of s-SWCNTs has not been reported when constituting a network at a given channel length, including the electrical characteristics of the networks. Therefore, it is significant to theoretically calculate the critical number of s-SWCNTs, which is required to constitute networks at a given channel length. For this reason, we calculated the percolation thresholds of s-SWCNT networks in the channels of FET, and the electrical characteristics of the networks. The Monte Carlo method was employed to generate random networks, and s-SWCNT networks were generated 100 times by varying the network densities at a given channel length to obtain the percolation probability of s-SWCNTs. Three channel lengths were used at a fixed channel width in the calculations. Moreover, we did not restrict the angle of the s-SWCNTs with respect to the horizontal axis in random network generation. Relative neighbourhood graphs (RNG) represent the morphology of percolated s-SWCNT networks quite well; therefore, we employed the percolation threshold in a RNG to gain the electrical percolation thresholds of s-SWCNT networks. Then, SPICE simulation was carried out to predict the electrical characteristics of the percolated s-SWCNT networks, and the percolation thresholds of s-SWCNT networks were related to their electrical characteristics.

We believe that this work can provide a theoretical guideline in constructing s-SWCNT networks at a given FET channel length.

Computational procedure

To obtain the electrical percolation thresholds of s-SWCNT networks, 2 dimensional (2D) networks of s-SWCNTs were randomly distributed in the channels of a FET. The networks were generated by MATLAB code based on the Monte Carlo method. Fig. 1(a) shows a schematic illustration of a model system for 2D s-SWCNT networks in a FET. The electrical percolation threshold was calculated at three different channel lengths of 2, 6, and 10 μm, defined by the source–drain electrodes. The channel width was fixed to 2 μm in each calculation. In addition, the length of the s-SWCNT was 1 μm (standard deviation $\sigma = 0.1$), while the angles of the s-SWCNTs with respect to the horizontal axis were randomly determined to be aligned in all directions during the generation of

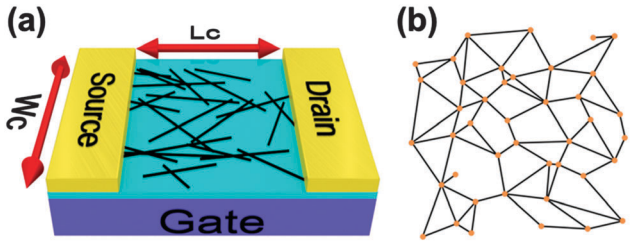

Fig. 1 (a) Schematic diagram of FET for percolation simulations of s-SWCNT networks. Sticks represent s-SWCNTs, which constitute networks between the source and drain electrodes on a dielectric layer of a substrate. Three different channel lengths (L_c, 2, 6, and 10 μm) were considered at a fixed channel width (W_c). (b) Illustration of the RNG, which represents percolated s-SWCNT networks quite well.

the networks. The length was determined by experimental results reporting that pure s-SWCNTs have length distributions centred at 1 μm.[29,30] To analyze the s-SWCNT networks with percolation theory, we employed bond percolation in a RNG, among diverse percolation models. This is because the RNG shown in Fig. 1(b) is geometrically quite similar to the 2D random networks of s-SWCNTs. To acquire the percolation probability of s-SWCNT networks, network generation was conducted 100 times at different network densities in each channel length. In addition, the number of s-SWCNTs for the network density was carefully decided so that the probability was distributed from 0 to 1 at each channel length. We defined the percolation threshold to be 0.77, because the bond percolation threshold of the RNG has been reported to be 0.77.[31]

Then, NGSPICE calculations were carried out to relate the percolation thresholds of the networks to the electrical characteristics of the s-SWCNT networks. For this, the information on network percolation was converted to an NGSPICE netlist file after finding connected electrical paths in the networks. In the SPICE calculations, each s-SWCNT was modeled as a simple p-type metal-oxide-semiconductor FET (MOSFET), because only s-SWCNTs were considered in this study. The junction resistance between the s-SWCNTs was carefully determined based on experimental reports on junction conductance between s-SWCNTs.[32] The study measured the junction conductance constituted by two individual s-SWCNTs to be $0.011e^2/h$ and $0.06e^2/h$ (where e is the electron charge and h is Planck's constant). From this, the junction resistances were calculated by inversing $0.011e^2/h$ and $0.06e^2/h$. As a result, the average of the calculated junction resistances was 1.4 MΩ, and this value was used in the SPICE simulation. The transfer characteristic curves of the s-SWCNT networks were obtained by sweeping the gate voltage from −3 to 3 V at a fixed source–drain voltage of 1 V. The on/off ratios of the networks were calculated using the ratio of the maximum to minimum current in the transfer characteristic curves obtained from percolated s-SWCNT networks.

Results and discussion

To obtain the percolation probability at each channel length, we generated s-SWCNT networks 100 times by using Monte

Carlo simulations at different s-SWCNT network densities. Fig. 2 shows the percolation probability of s-SWCNT networks with respect to network density at the channel lengths defined by the source–drain electrodes. Regardless of channel length, we can see a trend that the percolation probability becomes low at a sparse network density, whereas it increases at a high network density. However, the distribution of percolation probability has a different symmetry with respect to the network density, depending on channel length. Hence, we fitted the obtained data to the sigmoidal Boltzmann equation, which has the following form:

$$y = \frac{(A_1 - A_2)}{[1 + \exp(x - x_0)/\Delta x]} + A_2$$

where y is the percolation probability of the s-SWCNT network, x is the network density, A_1 is the initial value of y, A_2 is the final value of y and x_0 and Δx are the centre and the width of the function, respectively. The fitting parameters are summarized in Table 1 with adjusted R^2 values. As can be seen in the table, all adjusted R^2 values are close to 1, meaning that the fitting to the sigmoidal Boltzmann equation is quite appropriate. We can see in Fig. 2 that x_0 shifts to a region of high network density as the channel length increases. Especially, the table shows that an abrupt increase in x_0 occurs when the channel length changes from 2 to 6 μm. Although we used the same interval for the channel length, this value is greater than the difference between 6 and 10 μm. This can be attributed to the length of the s-SWCNTs (1 μm) considered in this work. Because the length of an individual s-SWCNT is half of the channel length in the case of 2 μm, the percolation probability of the s-SWCNT network increases even with a small number of s-SWCNTs, leading to sparse network density. On the other hand, the channel lengths of 6 and 10 μm are 6 and 10 times longer than the length of the s-SWCNTs, respectively. In both cases, a large number of s-SWCNTs is stochastically required to constitute s-SWCNT networks, compared with the 2 μm channel length. This is the reason why x_0 shifts to the right in the axis of network density as the channel length increases.

To obtain the percolation threshold at each channel length, we employed bond percolation in an RNG which represents the morphology of s-SWCNT percolation well. The percolation threshold in this RNG has been reported to be 0.77.[32] Hence, as shown in Fig. 2, we plotted a dashed line at a value of 0.77 in the axis of percolation probability. The network densities at the percolation threshold, calculated from the sigmoidal Boltzmann equation for channel lengths of 2, 6, and 10 μm, were 6.8, 9.0, and 9.9 tube μm^{-2}, respectively. To determine the relationship between network density and channel length, we plotted the network density at the percolation threshold against the channel length, as shown in Fig. 3. The figure shows that as the channel length increases, the network density corresponding to the percolation threshold of the s-SWCNT network increases logarithmically. As explained previously, the s-SWCNT network density abruptly increases when the channel length increases from 2 to 6 μm. This can be explained as follows: junctions in the channel of the FET can be classified as s-SWCNT to electrode and s-SWCNT to s-SWCNT contacts. When s-SWCNTs contact the electrode in the FET, a junction forms between one- and two-dimensional structures. Meanwhile, the contact between s-SWCNT and s-SWCNT is a junction consisting of one-dimensional structures. In general, we can predict a higher probability of contact between one- and two-dimensional structures than between one-dimensional ones. Therefore, the percolation probability of forming networks decreases as the channel length increases. In other words, more s-SWCNTs are required to compensate for the low contact probability between the s-SWCNTs, covering the increased area by the extension of the channel length.

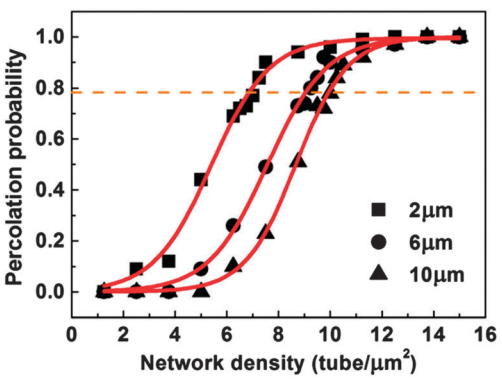

Fig. 2 Plot of percolation probability *versus* network density at channel lengths of 2, 6, and 10 μm. A dashed line was placed at the percolation probability of 0.77, which corresponds to the percolation threshold in the RNG. The network density at the percolation threshold increases with increasing channel length.

Table 1 Fitting parameters for sigmoidal Boltzmann analysis at each channel length

	2 μm	6 μm	10 μm
A_1	0	0	0
A_2	0.9945	0.9982	1.0
X_0	5.3964	7.5657	8.6672
Δx	1.1157	1.1461	0.9876
Adjusted-R^2	0.9927	0.9967	0.9980

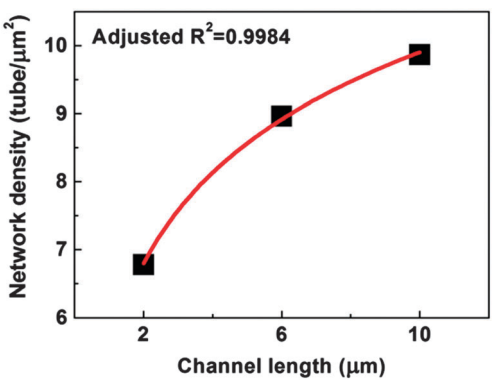

Fig. 3 Effect of channel length on the network density at the percolation threshold. The network density at the percolation threshold increases with increasing channel length.

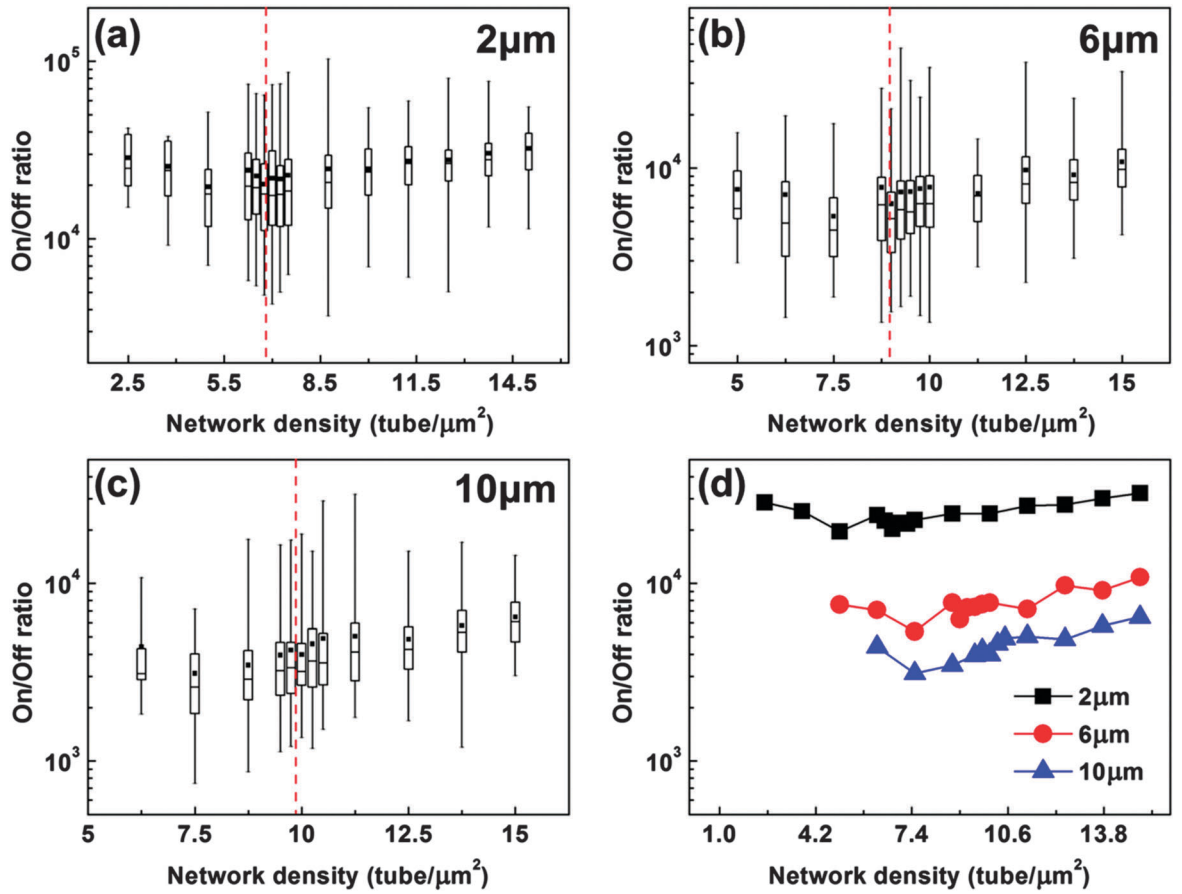

Fig. 4 Box plots of the on/off ratios of the percolated s-SWCNT networks *versus* network density at channel lengths of (a) 2, (b) 6, and (c) 10 μm. The on/off ratio is enhanced in all cases as the network density increases. The average on/off ratios of percolated s-SWCNTs are summarized with respect to network density, as shown in (d). The squares, circles, and triangles represent the changes in the average on/off ratios with respect to network density at channel lengths of 2, 6, and 10 μm, respectively.

After generating s-SWCNT networks at each channel length, transfer characteristics were obtained from percolated s-SWCNT networks by a SPICE simulator. At each channel, the on/off ratio of the FET was calculated from all percolated networks, and the results are displayed in Fig. 4(a)–(c) as box plots against network density. A dotted line was placed at the network density corresponding to the percolation threshold of the s-SWCNT networks, and the average on/off ratio was marked with a closed square in all cases. In each case, we can see that the on/off ratio is enhanced as the network density increases. This result is different from previous results, where m-SWNCT and s-SWCNT co-exist in percolated networks.[15] When s-SWCNT and m-SWCNT coexist, the on/off ratio rapidly decreases in dense SWCNT networks due to the metallic path created by the m-SWCNTs. The m-SWCNT path becomes electrically dominant in the SWCNT networks when a voltage is applied. Therefore, we cannot expect semiconducting behavior originating from percolated s-SWCNT networks.

In the case of the 2 μm channel length (Fig. 4(a)), we can observe that the difference between the maximum and the minimum on/off ratios gradually decreases above the percolation threshold. This is because the percolation probability approaches 1 as the number of s-SWCNTs increases, leading to a narrow distribution of the on/off ratios. Fig. 4(b) exhibits the box plot corresponding to the channel length of 6 μm. It seems that the difference between the maximum and the minimum is not as great as shown in Fig. 4(a). Moreover, we can see that the on/off ratio is slightly enhanced with increasing network density. However, the box plot for the 10 μm channel length shows a different trend in that the difference between the maximum and the minimum of the on/off ratio varies unevenly with increasing network density. This is because the extended channel length gives a high probability that the percolated networks will have a different number of junctions and paths in spite of the high network density. To investigate the effect of network density on the on/off ratio, we plotted the average on/off ratios of all channels in the same figure, as exhibited in Fig. 4(d). As shown in the figure, the on/off ratio slightly increases above the percolation threshold in all cases with increasing network density. Therefore, we can conclude that the on/off ratio has a proportional relationship to the network density of s-SWCNTs. Moreover, In Fig. 4(d), we can observe that the on/off ratio decreases as the channel length increases. This figure indicates that when the channel length is 2 μm, we can expect

an on/off ratio of more than 10^4 regardless of network density. On the other hand, the on/off ratio has a value between 10^3 and 10^4 when the channel length is greater than 2 μm. Based on this result, it can be deduced that the on/off ratio of s-SWCNT is dependent on the channel length of the FET.

In general, the value of the on/off ratio can be determined by dividing the maximum of the on-state current by the minimum of the off-state current. In addition, the current from s-SWCNT networks is influenced by the number of junctions and electrical paths in the networks. Therefore, investigation of the percolation morphology of s-SWCNTs is significant to compare the difference in the number of junctions at different channel lengths and network densities. In Fig. 5, we illustrated representative percolation morphologies selected near the threshold network density and from the region of high network density. The number of electrical paths in the percolated networks commonly increases in all channel lengths as the network density increases. At a fixed network density, the number of junctions increases in proportion to the channel length, as shown in Fig. 5. This increase leads to the enhancement of junction resistance in the s-SWCNT networks, and influences the on- and off-state currents of the FET.

Hence, we analyzed the average on-state current and off-state current in all cases to clarify the dependency of the on/off ratio on channel length. Fig. 6(a) and (b) exhibit a plot of the average off-state and on-state currents with respect to the network density of s-SWCNTs, respectively. Interestingly, it seems that the off-state current is not affected by channel length, and maintains a similar value regardless of channel length, as seen in Fig. 6(a). In all channel lengths, the off-state current linearly increases in proportion to the network density. It can be interpreted that the resistance of an individual s-SWCNT is much higher than the junction resistance, and that the effect of junction resistance is insignificant. On the other hand, Fig. 6(b) evidently shows that the on-state current decreases as the channel length increases. This can be attributed to the junction resistance of s-SWCNT networks. As the channel length increases, the number of s-SWCNTs also increases to constitute an electrical path between the source–drain electrodes of the FET. This means that the number of junctions in the networks also increase with increasing channel length. Therefore, a longer channel contributes to the enhancement of junction resistance, and this causes the on-state current to decrease. As a result, the on/off ratio decreases with increasing channel length.

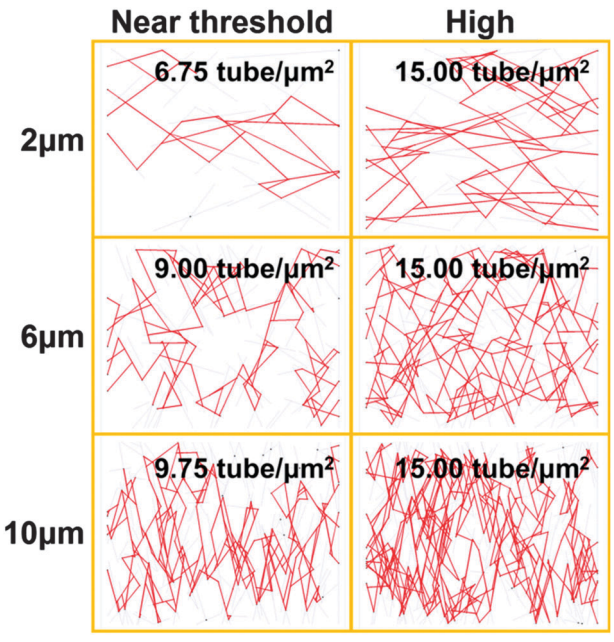

Fig. 5 Representative percolation morphologies of s-SWCNT networks at different channel lengths and network densities. The increase in network density as well as channel length leads to an increased number of electrical paths and contact junctions.

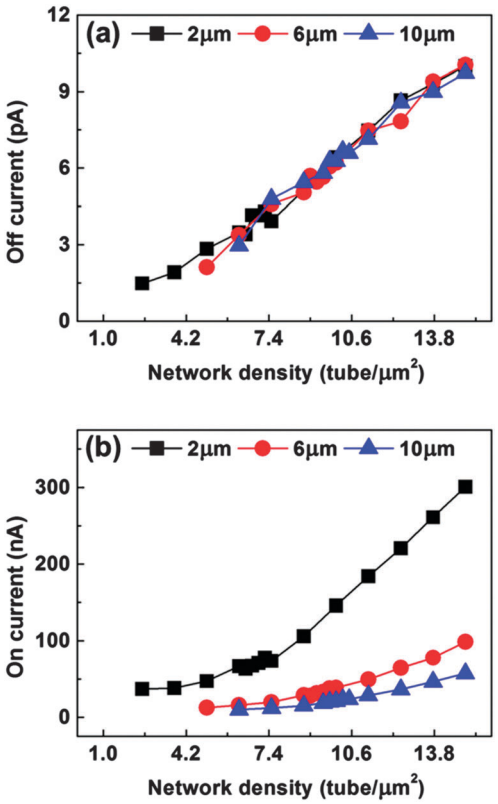

Fig. 6 Plot of average (a) off-state and (b) on-state currents *versus* network density at channel lengths of 2 (square), 6 (circle), and 10 μm (triangle).

Next, we investigated a relationship between the percolation threshold and the electrical characteristics at each channel length. As an analytic variable, we selected the network density at a percolation threshold of 0.77 for all channel lengths. In addition, the average on/off ratio was selected as a variable for the electrical characteristics of s-SWCNT networks. Fig. 7 exhibits the change in the average on/off ratio with respect to the network density at the percolation threshold. The following formula was employed for the relationship between the average on/off ratio and the network density:

$$(\text{on/off})_{\text{avg}} = b \times (\text{Network density})^a$$

A power law model was used to fit the data, and the fitting parameters of a and b were -4.22 and 7.0×10^7, respectively.

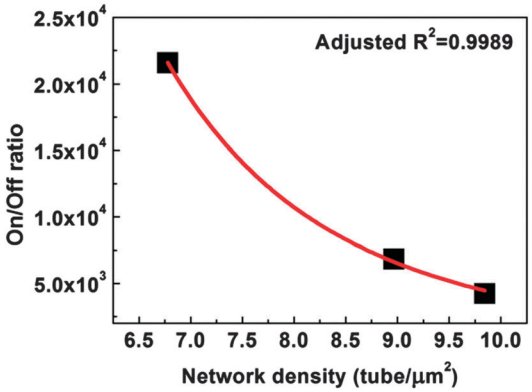

Fig. 7 Relationship between the average on/off ratio and network density corresponding to the percolation threshold of s-SWCNT networks at each channel. At the percolation threshold, the on/off ratios of s-SWCNT networks drastically decrease with respect to network density.

The adjusted R^2 value was 0.9989, which is close to 1. This indicates that the on/off ratio is strongly influenced by the network density at the percolation threshold. The on/off ratio drastically decreases as the network density at the percolation threshold in each channel length increases. Notably, although the channel length increases at the same interval, a sudden decrease in the on/off ratio occurs between the network densities corresponding to the percolation thresholds of the 2 and 6 μm channel lengths. It can be demonstrated that at the percolation threshold of each channel, more s-SWCNTs are necessary to constitute networks between electrodes with increased channel lengths. Simultaneously, the number of junctions between the s-SWCNTs grows in s-SWCNT networks, leading to the enhancement of junction resistance. Finally, a low on/off ratio is obtained for s-SWCNT networks formed in extended channel lengths. To analyze our results, the MOSFET model theory was employed. When MOSFET is switched on, the drain current (I_D) generally depends on the dimensions of the channel length and channel width. In this study, the channel width was fixed to 2 μm in all cases.

$$I_D \propto \frac{\text{Channel width}}{\text{Channel length}}$$

Therefore, we can see that I_D has an inversely proportional relationship to channel length. On the other hand, I_D is not influenced by channel dimension when MOSFET is switched off. From this relationship, we can expect that the on/off ratio decreases in inverse proportion to the channel length. As shown in Fig. 7, our result is consistent with the MOSFET model.

Conclusions

In this work, we theoretically obtained the percolation thresholds of s-SWCNT networks at different channel lengths on the basis of the Monte Carlo method. As a result, the percolation thresholds of the s-SWCNT networks were calculated to be 6.8, 9.0, and 9.9 tube μm^{-2} when the channel lengths were 2, 6, and 10 μm, respectively. The network density gained at the percolation threshold of s-SWCNT increased with respect to channel length. In addition, we predicted the electrical characteristics of percolated s-SWCNT networks at each channel length by using a SPICE simulator. It was revealed that the on/off ratio was slightly enhanced with increasing network density for all channel lengths. Finally, we found a power law relationship between the on/off ratio and the network density at the percolation threshold of the s-SWCNT networks. This originated from the reduction of the on-state current due to the enhanced junction resistance caused by extending the channel length of the FET.

This study can provide a theoretical guideline when generating CNT networks, as well as s-SWCNT networks at a given channel length of FET.

Acknowledgements

This work was supported by BK21 Humanware Information Technology and the Center for Advanced Soft Electronics under the Global Frontier Research Program of the Ministry of Education (No. 2011-0031638).

Notes and references

1 S. Iijima, *Nature*, 1991, **354**, 56–58.
2 X. Zhou, J.-Y. Park, S. Huang, J. Liu and P. L. McEuen, *Phys. Rev. Lett.*, 2005, **95**, 146805.
3 J. W. Mintmire, B. I. Dunlap and C. T. White, *Phys. Rev. Lett.*, 1992, **68**, 631–634.
4 R. Saito, M. Fujita, G. Dresselhaus and M. S. Dresselhaus, *Phys. Rev. B: Condens. Matter Mater. Phys.*, 1992, **46**, 1804–1811.
5 N. Hamada, S.-I. Sawada and A. Oshiyama, *Phys. Rev. Lett.*, 1992, **68**, 1579–1581.
6 B. I. Dunlap, *Phys. Rev. B: Condens. Matter Mater. Phys.*, 1994, **49**, 5643–5650.
7 M. Menon, E. Richter and K. R. Subbaswamy, *J. Chem. Phys.*, 1996, **104**, 5875–5882.
8 D. Zhang, K. Ryu, X. Liu, E. Polikarpov, J. Ly, M. E. Tompson and C. Zhou, *Nano Lett.*, 2006, **6**, 1880–1886.
9 B. Dan, G. C. Irvin and M. Pasquali, *ACS Nano*, 2009, **3**, 835–843.
10 R. Ulbricht, S. B. Lee, X. Jiang, K. Inoue, M. Zhang, S. Fang, R. H. Baughman and A. A. Zakhidov, *Sol. Energy Mater. Sol. Cells*, 2007, **91**, 416–419.
11 M. Zheng, A. Jagota, M. S. Strano, A. P. Santos, P. Barone, S. G. Chou, B. A. Diner, M. S. Dresselhaus, R. S. McLean, G. B. Onoa, G. G. Samsonidze, E. D. Semke, M. Usrey and D. J. Walls, *Science*, 2003, **302**, 1545–1548.
12 T. Tanaka, H. Jin, Y. Miyata, S. Fujii, H. Suga, Y. Naitoh, T. Minari, T. Miyadera, K. Tsukagoshi and H. Kataura, *Nano Lett.*, 2009, **9**, 1497–1500.
13 M. S. Arnold, A. A. Green, J. F. Hulvat, S. I. Stupp and M. C. Hersam, *Nat. Nanotechnol.*, 2006, **1**, 60–65.
14 L. Qu, F. Du and L. Dai, *Nano Lett.*, 2008, **8**, 2682–2687.
15 J. Li, Z.-B. Zhang and S.-L. Zhang, *Appl. Phys. Lett.*, 2007, **91**, 253127.
16 F. Du, J. E. Fischer and K. I. Winey, *Phys. Rev. B: Condens. Matter Mater. Phys.*, 2005, **72**, 121404.

17 S. Pfeifer, S.-H. Park and P. R. Bandaru, *J. Appl. Phys.*, 2010, **108**, 024305.
18 V. K. Sangwan, A. Behnam, V. W. Ballarotto, M. S. Fuhrer, A. Ural and E. D. Williams, *Appl. Phys. Lett.*, 2010, **97**, 043111.
19 B. Chandra, H. Park, A. Maarouf, G. J. Martyna and G. S. Tulevski, *Appl. Phys. Lett.*, 2011, **99**, 072110.
20 M. Berahman, M. Taheri, M. H. Sheikhi and A. Zarifkar, 21st Iranian Conference on, Electrical Engineering (ICEE), Mashhad, 14–16 May, 2013, DOI: 10.1109/IranianCEE.2013.6599543.
21 N. Izard, S. Kazaoui, K. Hata, T. Okazaki, T. Saito, S. Iijima and N. Minami, *Appl. Phys. Lett.*, 2008, **92**, 243112.
22 D.-H. Kim, J. K. Lee, J. H. Huh, Y. H. Kim, G. T. Kim, S. Roth and U. Dettlaff-Weglikowska, *Phys. Status Solidi B*, 2011, **248**, 2668–2671.
23 D.-H. Kim, S. Y. Lee, J. E. Jin, G. T. Kim and D.-J. Lee, *Phys. Chem. Chem. Phys.*, 2014, **16**, 6980–6985.
24 D.-H. Kim, J. E. Jin, M. Piao, J. H. Choi and G. T. Kim, *Phys. Chem. Chem. Phys.*, 2014, **16**, 18370–18374.
25 S. Fujii, T. Tanaka, Y. Miyata, H. Suga, Y. Naitoh, T. Minari, T. Miyadera, K. Tsukagoshi and H. Kataura, *Appl. Phys. Express*, 2009, **2**, 071601.
26 S. K. Raman Pillai and M. B. Chan-Park, *ACS Appl. Mater. Interfaces*, 2012, **4**, 7047–7054.
27 K. C. Narasimhamurthy and P. Roy, *Semicond. Sci. Technol.*, 2011, **26**, 075002.
28 K. C. Narasimhamurthy and R. Paily, *Solid-State Electron.*, 2013, **79**, 37–44.
29 B. K. Sarker, S. Shekhar and S. I. Khondaker, *ACS Nano*, 2011, **5**, 6297–6305.
30 C. Wang, J. Zhang and C. Zhou, *ACS Nano*, 2010, **4**, 7123–7132.
31 O. Melchert, *Phys. Rev. E: Stat. Phys., Plasmas, Fluids, Relat. Interdiscip. Top.*, 2013, **87**, 042106.
32 M. S. Fuhrer, J. Nygård, L. Shih, M. Forero, Y.-G. Yoon, M. S. C. Mazzoni, H. J. Choi, J. Ihm, S. G. Louie, A. Zettl and P. L. McEuen, *Science*, 2000, **288**, 494–497.

